Heliyon 9 (2023) e22857

Contents lists available at ScienceDirect

Heliyon

journal homepage: www.cell.com/heliyon

Oxidative stress drives vascular smooth muscle cell damage in acute Stanford type A aortic dissection through HIF-1α/HO-1 mediated ferroptosis

Wenyu Song [a,1], Yifu Chen [b,1], Lieyang Qin [a,1], Xinyuan Xu [c,1], Yu Sun [b], Mingzhu Zhong [b], Yuntao Lu [a], Kui Hu [d], Lai Wei [a,**], Jinmiao Chen [a,*]

[a] Department of Cardiovascular Surgery, Zhongshan Hospital, Fudan University, Shanghai 200032, China
[b] Institute of Neuroscience, Center for Excellence in Brain Science and Intelligence Technology, Chinese Academy of Sciences, Shanghai 200031, China
[c] The Second Clinical Medical School, Nanjing Medical University, Nanjing 210029, China
[d] Department of Cardiovascular Surgery, Guizhou Provincial People's Hospital, Guiyang 550002, China

ARTICLE INFO

Keywords:
Acute Stanford type A aortic dissection
Vascular smooth muscle cell
Ferroptosis
HO-1
HIF-1α

ABSTRACT

Background: Acute Stanford type A aortic dissection (ATAAD) is characterized by intimal tearing and false lumen formation containing large amounts of erythrocytes with heme. Heme oxygenase 1 (HO-1) is the key enzyme to degrade heme for iron accumulation and further ferroptosis. The current study aimed at investigating the role of HO-1 in the dissection progression of ATAAD.
Methods: Bioinformatic analyses and experimental validation were performed to reveal ferroptosis and HO-1 expression in ATAAD. Human aortic vascular smooth muscle cell (HA-VSMC) was used to explore underlying molecular mechanisms and the role of HO-1 overexpression in ATAAD.
Results: Ferroptosis was identified as a critical manner of regulated cell death in ATAAD. HO-1 was screened as a key signature of ferroptosis in ATAAD, which was closely associated with oxidative stress. Single cell/nucleus transcriptomic analysis and histological staining revealed that HO-1 and HIF-1α were upregulated in vascular smooth muscle cell (VSMC) of ATAAD. Further in vitro experiments showed that H_2O_2-induced oxidative stress increased VSMC ferroptosis with the overexpression of HO-1, which could be suppressed by HIF-1α inhibitor PX-478. HIF-1α could transcriptionally regulate the expression of HO-1 through binding to its promoter region. Pharmacological inhibition of HO-1 by zinc protoporphyrin (ZnPP) did not reduce H_2O_2-induced HA-VSMC damage without heme co-incubation. However, H_2O_2-induced HA-VSMC damage was worsened when heme was added into the medium, and ZnPP could reduce HA-VSMC damage in this condition.
Conclusion: HO-1 is a key signature of VSMC ferroptosis in ATAAD. HIF-1α/HO-1 mediated ferroptosis might participate in oxidative stress induced VSMC damage.

* Corresponding author.
** Corresponding author.
E-mail addresses: wei.lai@zs-hospital.sh.cn (L. Wei), chen.jinmiao@zs-hospital.sh.cn (J. Chen).
[1] These authors contributed equally to this work.

https://doi.org/10.1016/j.heliyon.2023.e22857
Received 10 May 2023; Received in revised form 16 November 2023; Accepted 21 November 2023
Available online 26 November 2023

1. Introduction

Thoracic aortic aneurysm and dissection is a life-threatening cardiovascular disease with high risk of mortality with annual incidence of 6–16 per 100,000 [1]. Ascending thoracic aortic aneurysm (ATAA) and acute Stanford type A aortic dissection (ATAAD) are two subtypes of thoracic aortic diseases based on shared histopathologic feature of medial layer degeneration [2]. However, ATAA is characterized by chronic and progressive weakening and dilation of ascending thoracic aortic walls, while ATAAD is acute intimal tearing and dissection involving the ascending aorta.

Unlike ATAA, ATAAD is characterized by intimal tearing and acute false lumen formation. With the progression of false lumen, multiple complications might occur, including aortic valve insufficiency, tamponade, and even aortic rupture. Compared with type B aortic dissection, ATAAD is more life-threatening and requires urgent surgical repair [1,3]. In current era, mortality rate of ATAAD still remains as high as 23.7 % within 48 h after onset [4]. False lumen formation plays a key role in the dissection progression of ATAAD. It has been reported that larger size of false lumen predicts poor prognosis of ATAAD [5]. Currently, the progression of false lumen is mainly explained by physical tearing in an antegrade and retrograde manner. However, underlying molecular mechanisms of how false lumen progressed remains largely unknown. Better understanding of this process could provide novel insights into controlling the progression of false lumen after ATAAD onset.

Vascular smooth muscle cell (VSMC) damage and death may play an important role in the microenvironment of false lumen [2]. Besides apoptosis and necrosis, several new manners of regulated cell death (RCD) have been discovered in recent years, including cuproptosis, ferroptosis, necroptosis, autophagy, immunogenic cell death (ICD), and pyroptosis [6]. Notably, ferroptosis is a kind of RCD based on iron accumulation and lipid peroxidation [7]. Thrombus within false lumen of ATAAD contains large amounts of erythrocytes with heme. Heme oxygenase (HO) is the key enzyme in heme catabolism to produce iron for ferroptosis. HO-1, a major type of HO, is strongly induced in response to hypoxia, oxidative stress, and other internal environmental shifts [8]. HO-1 plays an essential role in the pathogenesis of several cardiovascular disorders such as atherosclerosis and ischemic cardiomyopathy [9]. However, the role of HO-1 in ATAAD has not been fully understood. This study aimed at investigating how HO-1 functions in ATAAD, especially in oxidative stress-induced VSMC damage.

2. Methods and materials

2.1. Clinical specimens and ethics statement

A total of 96 aortic specimens were integrated and analyzed in this study, including 81 specimens from Gene Expression Omnibus (GEO) database and 15 clinical specimens from our center. Study protocols involving clinical specimens from patients were reviewed and approved by Ethical Committee of Zhongshan Hospital, Fudan University (Ethical number: B2022-374R). Written informed consent for experimentation was obtained from all patients. A total of 5 control, 5 ATAA and 5 ATAAD specimens were retrieved from patients undergoing open cardiac surgery. Control ascending thoracic aorta was obtained from recipient or donor of heart transplantation. For ATAA and ATAAD, patients were diagnosed according to the guideline [1], and were excluded if they had hereditary aortic disease (i.e., Marfan syndrome and Loeys-Dietz syndrome), iatrogenic injury, infection, and trauma.

2.2. Public transcriptome data acquisition and preprocessing

Transcription data of human ATAAD were obtained from the open-source GEO database (https://www.ncbi.nlm.nih.gov/geo/) including high throughput sequencing datasets (GSE107844, GSE147026, GSE153434) and a microarray dataset (GSE52093). Transcription dataset GSE140947 of human ATAA was also downloaded from GEO database. The details of public transcriptional datasets were available at **Supplementary File 1**.

High throughput sequencing datasets GSE153434 and GSE107844 were combined as test group. Batch effect was eliminated with R function 'ComBat' from R package 'sva' (Version 3.42.0) through empirical Bayesian theory [10]. R function 'prcomp' was used to perform PCA to confirm the effect of batch-normalized data. For combination of ATAA and ATAAD samples, merged GSE153434 and GSE107844 were combined with ATAA dataset GSE140947, with elimination of batch effect as described above. Another high throughput dataset GSE147026 and microarray dataset GSE52093 were independently used as validation datasets.

2.3. Differential analysis

We performed differential analysis for screening differentially expressed genes (DEGs) between ATAAD and control specimens using R package 'limma' (Version 3.50.0). Genes with an average transcriptional value lower than 0.5 were filtered and excluded. R function 'wilcox.test' was used for screening DEGs after overall checking data distributions. $|\log FC| > 1$ and P value < 0.05 were set as the cut-off value to identity DEGs [11]. Heatmap of gene expression was plotted with a Z-score standardization [12].

2.4. Protein-protein interaction (PPI) network

Interested gene list was uploaded to STRING database (https://cn.string-db.org/) to construct networks and analyze protein functional interaction relationships [13]. Then, networks were uploaded to Cytoscape (Version 3.9.1) for visualization [14].

2.5. Gene ontology (GO) analysis

GO enrichment analysis was further performed based on DEGs to reveal the difference of biofunction between groups including biological process (BP), cellular component (CC), and molecular function (MF) [15]. This process was performed using R packages 'clusterProfiler' (Version 4.2.0), 'org.Hs.eg.db' (Version 3.14.0), 'enrichplot' (Version 1.14.0) and 'ggplot2' (Version 3.3.5).

2.6. Gene set enrichment analysis (GSEA) and single sample gene set enrichment analysis (ssGSEA)

In this study, six different manners of RCD were focused and analyzed including autophagy, cuproptosis, ferroptosis, ICD, necroptosis and pyroptosis. First, we obtained gene lists involving in these six RCD from high-quality literatures, including 847 autophagy related genes (ARG) [16], 10 cuproptosis related genes (CRG) [17], 61 ferroptosis related genes (FRG) [7], 28 ICD related genes (IRG) [18], 52 necroptosis related genes (NRG) [19] and 51 pyroptosis related genes (PRG) [20]. We summarized these genes in **Supplementary File 2** as a reference dataset for GSEA and ssGSEA analysis.

GSEA was performed with 'gsea-3.0.jar' software. The number of permutations was set as 1000 as default. Multi-GSEA enrichment plots were described based on interested GSEA pathways using R package 'plyr' (Version 1.8.6), 'ggplot2', 'grid' (Version 4.1.1) and 'gridExtra' (Version 2.3). The significant threshold for GSEA analysis was set as 0.05 [21]. For ssGSEA, R packages 'GSVA' (Version 1.42.0) and 'GSEABase' (Version 1.56.0) were used to perform the analyses. Method was set as 'ssgsea' in R function 'gsva'. Enrichment scores were standardized with Min-Max method [22]. The average of enrichment scores was compared between groups and the significant threshold was 0.05 as default [23].

2.7. Hub gene screening based on machine learning algorithms

Two independent machine learning algorithms were used for hub gene screening including random forest [24] and support vector machine recursive feature elimination (SVM-RFE) [25]. For random forest algorithm, R package 'randomForest' was utilized to screen the hub genes from DEGs. Firstly, the optimal parameter 'mtry' was identified through the recurrent random forest classification for all possible variables (1–500). Secondly, each error rate of 1∼500 trees was calculated and the optimal parameter mtry was determined by the lowest error rate and best stability. The random forest classifier was then used to calculate the results based on the above-selected parameters. Finally, the DEGs with significant importance were selected as the hub candidate genes for subsequent analysis according to the Gini coefficient method. The R packages 'e1071' (Version 1.7-9), 'kernlab' (Version 0.9-29) and 'caret' (Version 6.0-90) were used to conduct SVM-RFE algorithm. The receiver operating characteristic (ROC) curve was plotted using the R package 'pROC' (Version 1.18.0).

2.8. Single cell/nucleus transcriptomic analysis

Single cell/nucleus transcriptomic analysis was performed on control, ATAA and ATAAD thoracic aortic tissues. We integrated three control and seven aneurysmal ascending aortas from GSE155468 including a total of 41,744 aortic cells. The GSE155468 dataset initially contained 11 samples [26]. However, the expression of HO-1 was not available in the sample GSM4704937, which was excluded in further single-cell transcriptomic analysis. Single-nucleus RNA sequencing was performed on one ATAAD specimen from our center using 10X genomics platform (NovelBio, Shanghai, China).

Single cell/nucleus transcriptomic analysis was performed using R package 'Seurat' [27]. Data was first filtered with the following criteria: 200 $<$ feature number $<$5000, percent of mitochondria genes $<$10 %. Then data was scaled with a log normalization. Scale factor was set as 10,000. High variable genes were reserved for further analysis with R function 'FindVariableFeatures'. Cells were dimensionally reduced through PCA and t-distribution stochastic neighbor embedding (TSNE). R function 'FindAllMarkers' was used to identify marker genes between different clusters. Interested genes were then visualized in a TSNE plot through R function 'FeaturePlot'.

2.9. Morphological assay

Aortic specimens were fixed with 4 % neutral-buffered formalin, dehydrated, embedded with paraffin, and cut into 5-μm sections [28]. For Prussian blue staining, a morphological detection manner to evaluate iron accumulation, sections were stained with Prussian blue (Powerful Biology, Wuhan, China) for 60 min. Nuclei was stained with 2 % nuclear solid red for 5 min. For immunostaining, sections were immersed in sodium citrate antigen retrieval solution (Solarbio, Beijing, China) at 95 °C for 5 min to perform heat-induced antigen retrieval process. Unspecific bounding was blocked by 1 % bovine serum albumin (BSA) dissolved in phosphate buffer saline (PBS) for 60 min at room temperature. The tissues on the sections were then covered with diluted primary antibodies dissolved in 1 % BSA. Immunohistochemistry (IHC) was performed using a DAB kit (Gene Tech, Shanghai, China). For immunofluorescence (IF) dual staining, the first primary antibody was stained using a TSA kit (AKOYA, Delaware, USA) and the second primary antibody was directly labeled with the fluorescence secondary antibody. Nuclei were stained with DAPI (Solarbio, Beijing, China). Sections were scanned using a VS-120 microscope (Olympus, Tokyo, Japan). The primary and secondary antibodies were listed in **Supplementary File 3**. Image J software (Version: 1.8.0, NIH, Bethesda, MD, USA, RRID: SCR_003070) was used to calculate positive area of Prussian staining and the integral optical density (IOD) of IHC staining.

2.10. Cell culture and treatment

Human aortic vascular smooth muscle cell (HA-VSMC, RRID: CVCL_4009) was cultured in Dulbecco's modified Eagle's medium (DMEM) with high glucose, 10 % fetal bovine serum (FBS) and antibiotics including penicillin and streptomycin (Gibco, Oakland, CA, USA). For induction of oxidative stress, HA-VSMC was serum starved overnight and hydrogen peroxide (H_2O_2) was dose-dependently (0, 12.5, 25, 50, 100, 200, 400, 800 and 1000 μM) added into the serum-starved HA-VSMC for 24 h [29].

Simultaneously, cells were treated with ferroptosis inhibitor liproxstatin-1 (Lip-1), HIF-1α inhibitor PX-478 or HO-1 inhibitor Zinc Protoporphyrin (ZnPP) (MCE, New Jersey, USA) for 24 h at a dose of 0.1, 1, and 10 μM dissolved in dimethyl sulfoxide (DMSO) according to the manufacturer's instructions and previous studies [30–32]. All cells were cultured in a 37 °C incubator with 5 % CO2. For induction of protective effect of ZnPP on HA-VSMC, heme (Sigma-Aldrich, St. Louis, MO, USA) was added into the medium at a concentration of 50 μM based on previous studies [33,34]. For MTT assay, cells were seeded into 96 well plates at a density of 1×10^4 cells per well. For Annexin V/7-AAD, Western blot and glutathione (GSH) assay, cells were seeded into 6 well plates at a density of 5×10^5 cells per well.

2.11. Cell viability assay and cell death assay

In this study, cell viability was measured through 3-(4,5-dimethylthiazol-2-yl)-2,5-diphenyltetrazolium bromide (MTT) and Annexin V/7-AAD assay [35]. For MTT assay, cultured cells were first planted into 96-well plates. MTT regent was added at a volume of 10 μL into each well (0.5 mg/mL, Sigma-Aldrich, St. Louis, MO, USA). The plate was incubated at 37 °C for 4 h. Medium was then removed from the plate. Finally, 100 μL DMSO was added into each well to dissolve the crystal. The absorbency at a wavelength of 492 nm was measured by a microplate reader (Allsheng, Hangzhou, China). For cell death assay, Annexin V/7-AAD assay was performed on a flow cytometer (BD Biosciences, USA) to detect the cellular fluorescence using an Annexin V-PE/7-AAD detection kit (Vazyme, Nanjing, China) according to the manufacturers' protocol.

2.12. Lipid peroxidation, GSH assay and labile iron pool analysis

Ferroptosis is marked by increased lipid peroxidation induced by iron overload and imbalance of GSH-oxidized glutathione (GSSG) antioxidant system [36]. In this study, intracellular iron was evaluated by labile iron pool analysis using Calcein AM method (Beyotime, China) as previously described [37]. Malondialdehyde (MDA) and GSH concentrations of tissue or cell lysate were measured following the manufacturers' protocols using lipid peroxidation assay kit (Beyotime, China) and GSH assay kit (Beyotime, China), respectively.

2.13. Western blotting

After culture and treatment, cells were lysed with ice-cold lysis buffer containing 50 mmol L^{-1} Tris–HCL (pH = 7.4), 1 % NP-40, 150 mmol L^{-1} NaCl, 1 mmol L^{-1} EDTA and 1 mmol L^{-1} phenylmethyl sulfonyl fluoride (PMSF) for 30 min. Lysates were centrifuged at 12,000 g for 15 min at 4 °C. The supernatants were collected, and the protein concentration was measured using coomassie brilliant blue (Solarbio, Beijing, China) [38]. Cell lysates were boiled in SDS sample at 95 °C for 10 min and run on a 10 % SDS–polyacrylamide gel (120V constant voltage in stacking gel for 20 min, 20 mA constant current in separating gel for 100 min). The proteins were then transferred onto polyvinylidene fluoride (PVDF) membranes (Millipore, Billerica, MA, USA) at 4 °C, 300 mA for 1.5 h. PVDF membranes were blocked with 5 % fat-free dry milk in TBST buffer (Tris-buffered saline with 0.1 % Tween 20) at room temperature for 1 h and then immersed in diluted primary antibodies at 4 °C overnight. The PVDF membranes were washed with TBST buffer and were incubated with secondary antibodies. The membranes were treated with enhanced chemiluminescence system (Millipore, Billerica, MA, USA) and pictured in automatic chemiluminescence image analysis system (Tanon, Shanghai, China). The primary and secondary antibodies were listed in **Supplementary File 3**. The bands were analyzed with Image J software.

2.14. Luciferase reporter gene assay

We predicted binding sites of HIF-1α in the promotor region of HO-1 from JASPAR database (http://jaspar.genereg.net/). The promotor region was defined as 2000 bases forward of the transcriptional start site (TSS) of the gene. The HIF-1α binding sites were identified as hypoxia response element (HRE). HO-1 promoter region was cloned forward of the luciferase reporter gene in a pGL3 basic vector (HO-1-promoter-luc, Genecreate, Wuhan, China). HIF-1α coding sequence was cloned in a pCAGGS basic vector for establishment of HIF-1α overexpression vector (Genecreate, Wuhan, China). For luciferase reporter gene assay, HA-VSMC cells were cultured at a density of 1×10^5 cells/well in 24 well culture plates. Cells were co-transfected with HO-1-promoter-luc and HIF-1α plasmid for 24 h using a Lipofectamine 3000 transfection kit (Invitrogen, Carlsbad, CA). The cells were lysed with 100 μL cold Glo lysis buffer (Promega, Fitchburg, WI, USA) for 5 min. Luciferase activity was detected using Luciferase Reporter Assay System (Promega, Fitchburg, WI, USA). Luciferase substrate was first diluted in PBS in a ratio of 1:3 and was added into 96 well in a volume of 100 μL with 10 μL cell lysates. The plate was read using a SpectraMax iD3 microplate reader (Molecular Devices, Shanghai, China).

2.15. Statistical analysis

R 4.1.3 and GraphPad Prism 9.0 software (San Diego, CA, USA) were applied to perform statistical analysis. All statistical analysis was performed based on characteristics and distributions of original data. Student's *t*-test was used for comparison between two groups if data obeyed normal distribution and homogeneity of variances. If not, Student's *t*-test with Welch's correction or Wilcoxon test was applied for comparison. Statistical analysis between multiple groups was performed through one-way ANOVA combined with Bonferroni correction [39]. Spearman's correlation was applied for correlation analysis. $P < 0.05$ was regarded as statistically significant.

3. Results

3.1. Ferroptosis is a critical manner of RCD in ATAAD

Transcriptome datasets from GEO database were downloaded for bioinformatic analysis. The flow chart of this part was available in

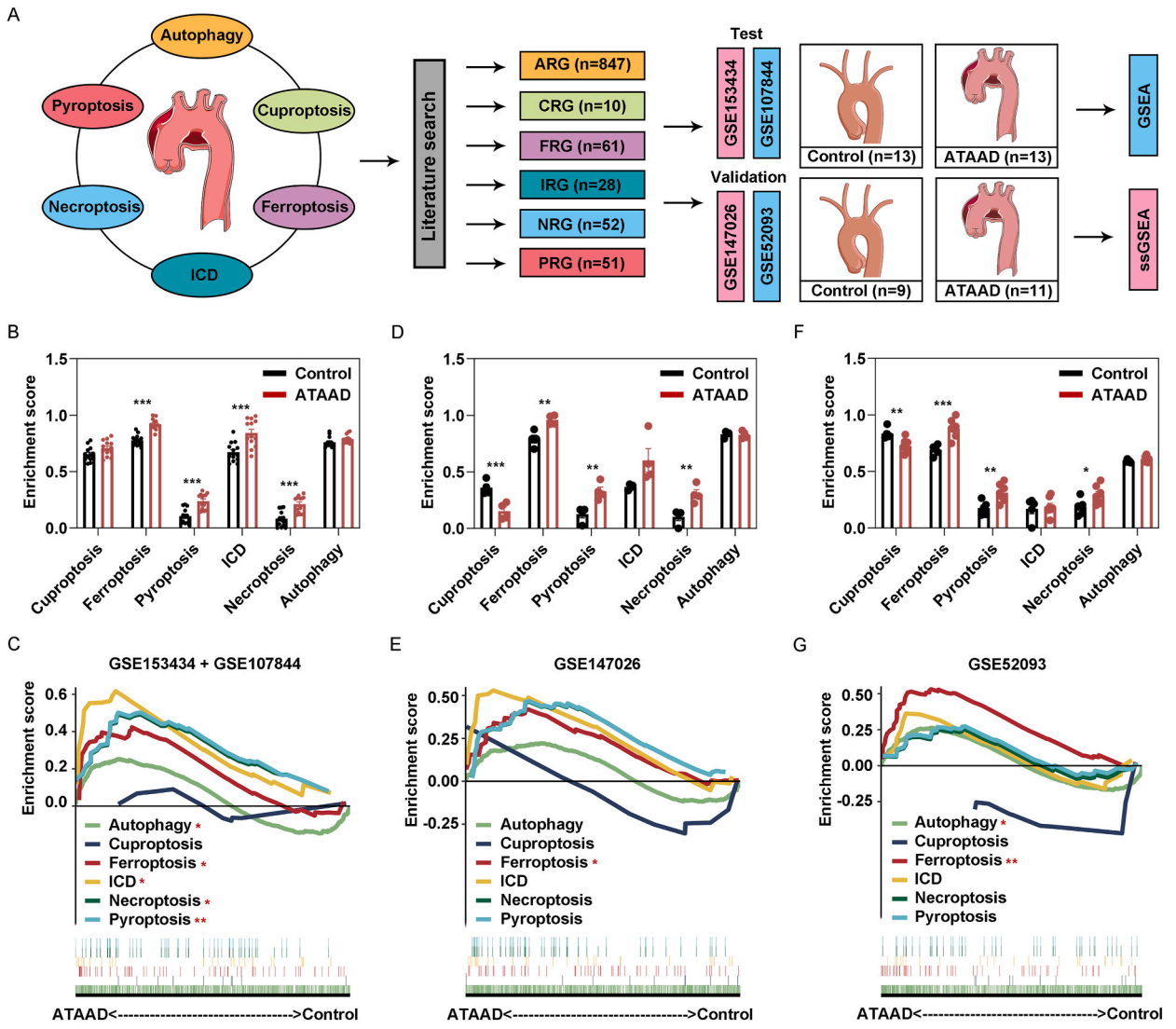

Fig. 1. Ferroptosis is Identified as a Critical Manner of RCD in ATAAD. (A) Flow chart of evaluating six manners of RCD in control and ATAAD ascending aorta. **(B–C)** Comparison of six manners of RCD in control and ATAAD of GSE153434 and GSE107844 through ssGSEA and GSEA. **(D–E)** Comparison of six manners of RCD in control and ATAAD of GSE147026 through ssGSEA and GSEA. **(F–G)** Comparison of six manners of RCD in control and ATAAD of GSE52093 through ssGSEA and GSEA. RCD, regulated cell death; ATAAD, acute Stanford type A aortic dissection; GSEA, gene set enrichment analysis; ssGSEA, single sample gene set enrichment analysis; ARG, autophagy related gene; CRG, cuproptosis related gene; FRG, ferroptosis related gene; IRG, immunogenic cell death related gene; NRG, necroptosis related gene; PRG, pyroptosis related gene. Data shown are means ± SEM. Statistical analysis was performed through Student's two-tailed *t*-test. $^{*}P < 0.05$, $^{**}P < 0.01$, $^{***}P < 0.001$.

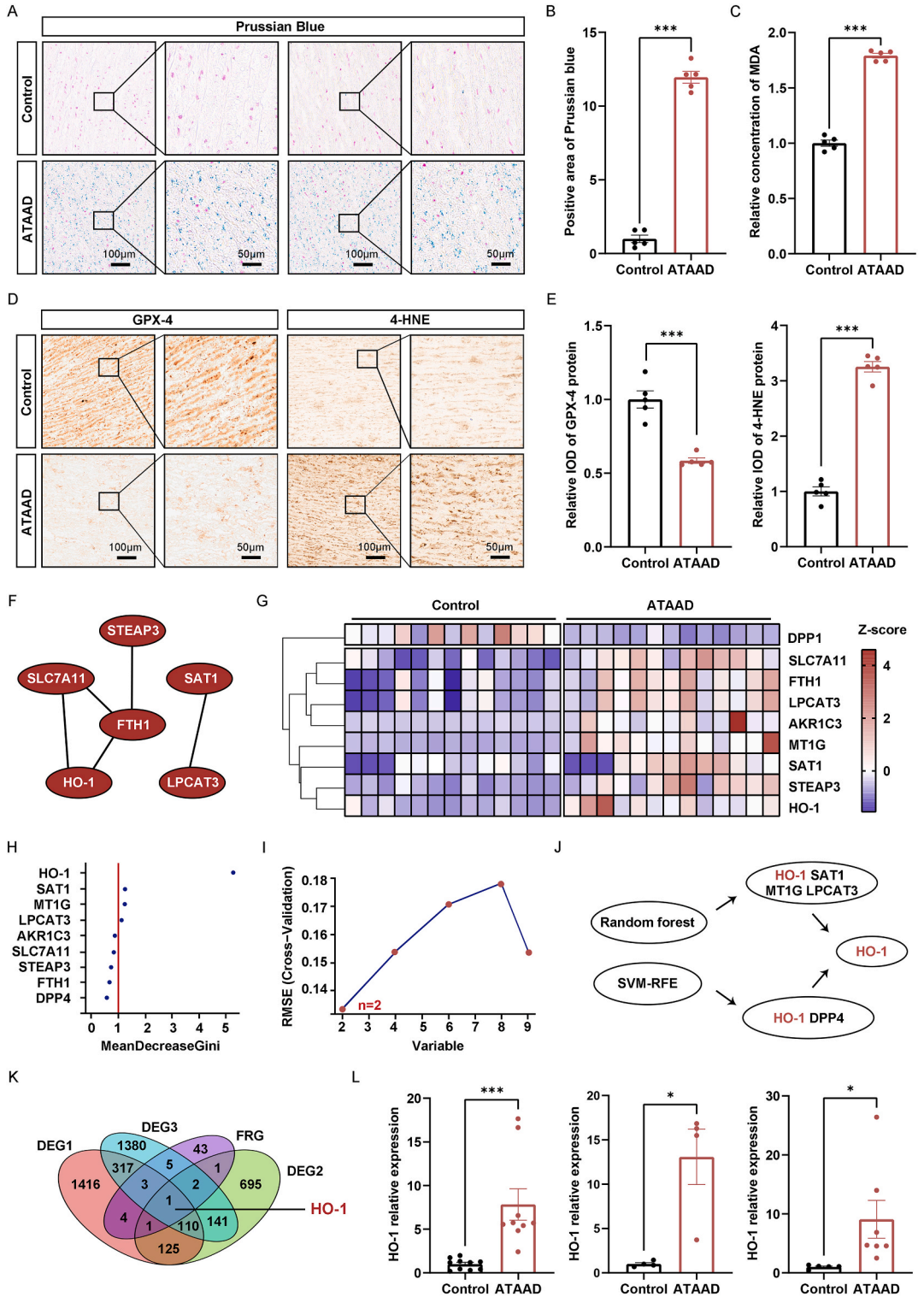

Fig. 2. Identification of HO-1 as a Key Signature of ATAAD through Machine Learning Algorithms. (A) Prussian blue staining in control and ATAAD. **(B)** Statistical analysis of Prussian blue staining. **(C)** MDA concentration in lipid peroxidation assay. **(D)** IHC staining of GPX-4 and 4-HNE in control and ATAAD. **(E)** Statistical analysis of GPX-4 and 4-HNE. **(F)** PPI network of differentially expressed FRGs from bioinformatic analysis. **(G)** Heatmap of differentially expressed FRGs between control and ATAAD thoracic aorta. Expression of FRGs in each specimen was normalized as z-scores. **(H)** Screening of key signature of ATAAD through random forest. **(I)** Screening of key signature of ATAAD through SVM-RFE. **(J)** Intersection of selected genes screened by random forest and SVM-RFE. **(K)** Intersection of DEGs and FRG. **(L)** Relative expression of HO-1 in control and ATAAD

of three datasets. HO-1, Heme oxygenase-1; MDA, malondialdehyde; PPI, protein-protein interaction network; SVM-RFE, support vector machine recursive feature elimination; DEG1, DEGs of GSE153434 and GSE107844; DEG2, DEGs of GSE147026; DEG3, DEGs of GSE52093; DEG, differentially expressed gene. Data shown are means ± SEM. Statistical analysis of morphological and lipid peroxidation assay were performed through Student's two-tailed *t*-test (Panel B, C and E). Statistical analysis of HO-1 expression was performed through Student's two-tailed *t*-test with Welch's correction (Panel L). $*P < 0.05$, $**P < 0.01$, $***P < 0.001$.

Fig. 1A. GSE153434 and GSE107844 were merged and further used as test datasets (13 control and 13 ATAAD). GSE147026 and GSE52093 were independently used as validation datasets (9 control and 11 ATAAD). GSEA and ssGSEA were performed to evaluate six manners of RCD in control and ATAAD ascending aorta.

In test datasets, we performed ssGSEA and found that ferroptosis, pyroptosis, ICD and necroptosis were significantly upregulated in ATAAD compared with control specimens (Fig. 1B). GSEA analysis showed that five manners of RCD were significantly enriched in ATAAD except cuproptosis (Fig. 1C). Validation dataset GSE147026 revealed an upregulation of ferroptosis, pyroptosis and necroptosis and a downregulation of cuproptosis (Fig. 1D). GSEA analysis only suggested significant enrichment of ferroptosis (Fig. 1E). Thus, ferroptosis was preliminarily identified as a critical RCD manner in ATAAD. Similar result was also observed with another validation dataset GSE52093 (Fig. 1F–G). Average enrichment scores of ferroptosis in ATAAD ranked first among these six manners of RCD in both test and validation datasets. With an integration and intersection, ferroptosis was screened as a prominent manner of RCD in ATAAD.

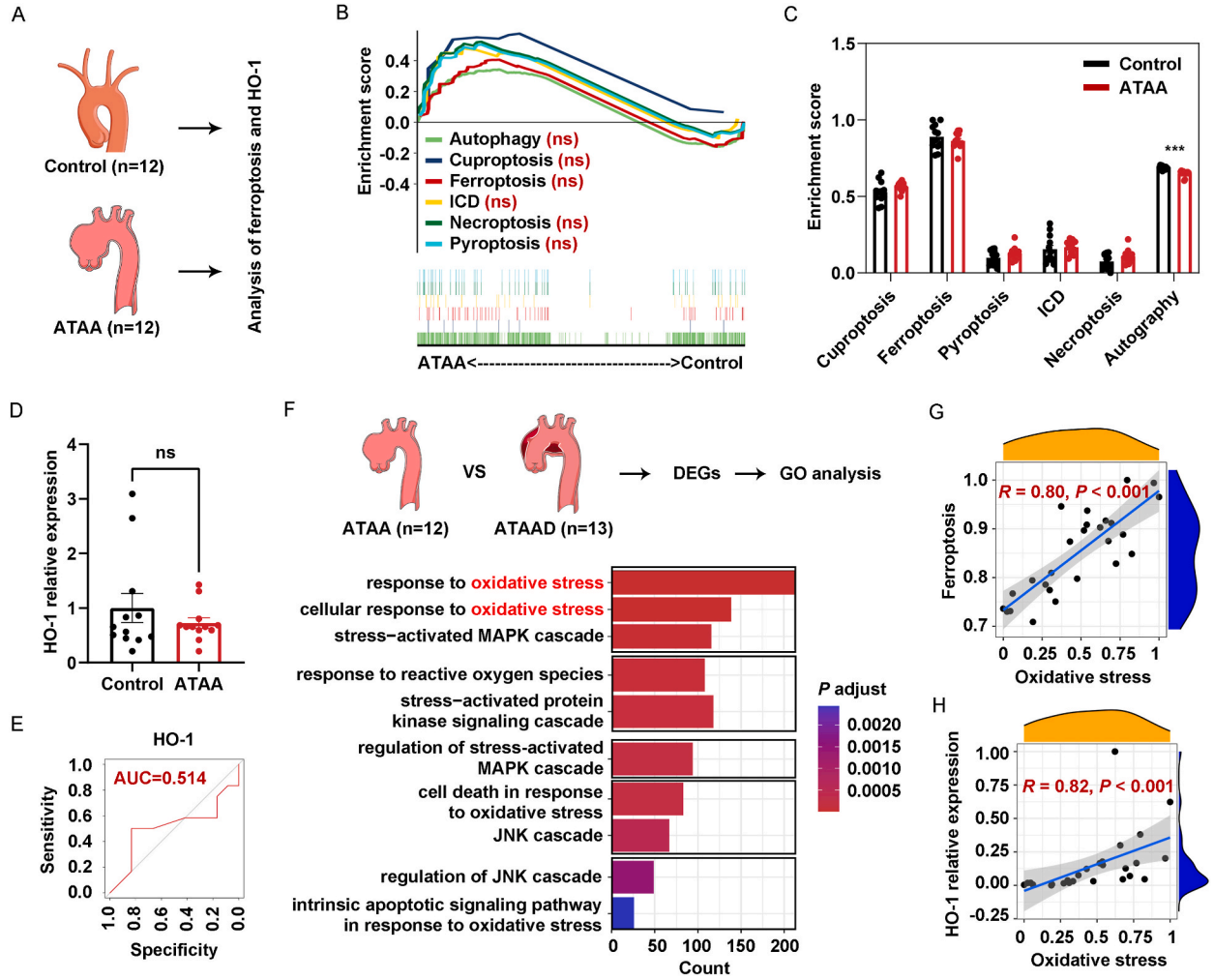

Fig. 3. Activation of Oxidative Stress is Significantly Associated with Ferroptosis and HO-1 expression in ATAAD. (A) Flow chart of analyses on ferroptosis and HO-1 based on GSE140947 of control and ATAA specimens. **(B)** GSEA of control and ATAA ascending aorta. **(C)** ssGSEA of control and ATAA ascending aorta. **(D)** Heatmap of HO-1 expression in control and ATAA ascending aorta. **(E)** GO analysis of ATAAD compared with ATAA. **(F)** Correlation analysis between oxidative stress and ferroptosis. **(G)** Correlation analysis between oxidative stress and HO-1 relative expression. ATAA, ascending thoracic aortic dissection; GO, gene ontology. Data shown are means ± SEM. Statistical analysis was performed through Student's two-tailed *t*-test (Panel C). $***P < 0.001$, ns = not significant.

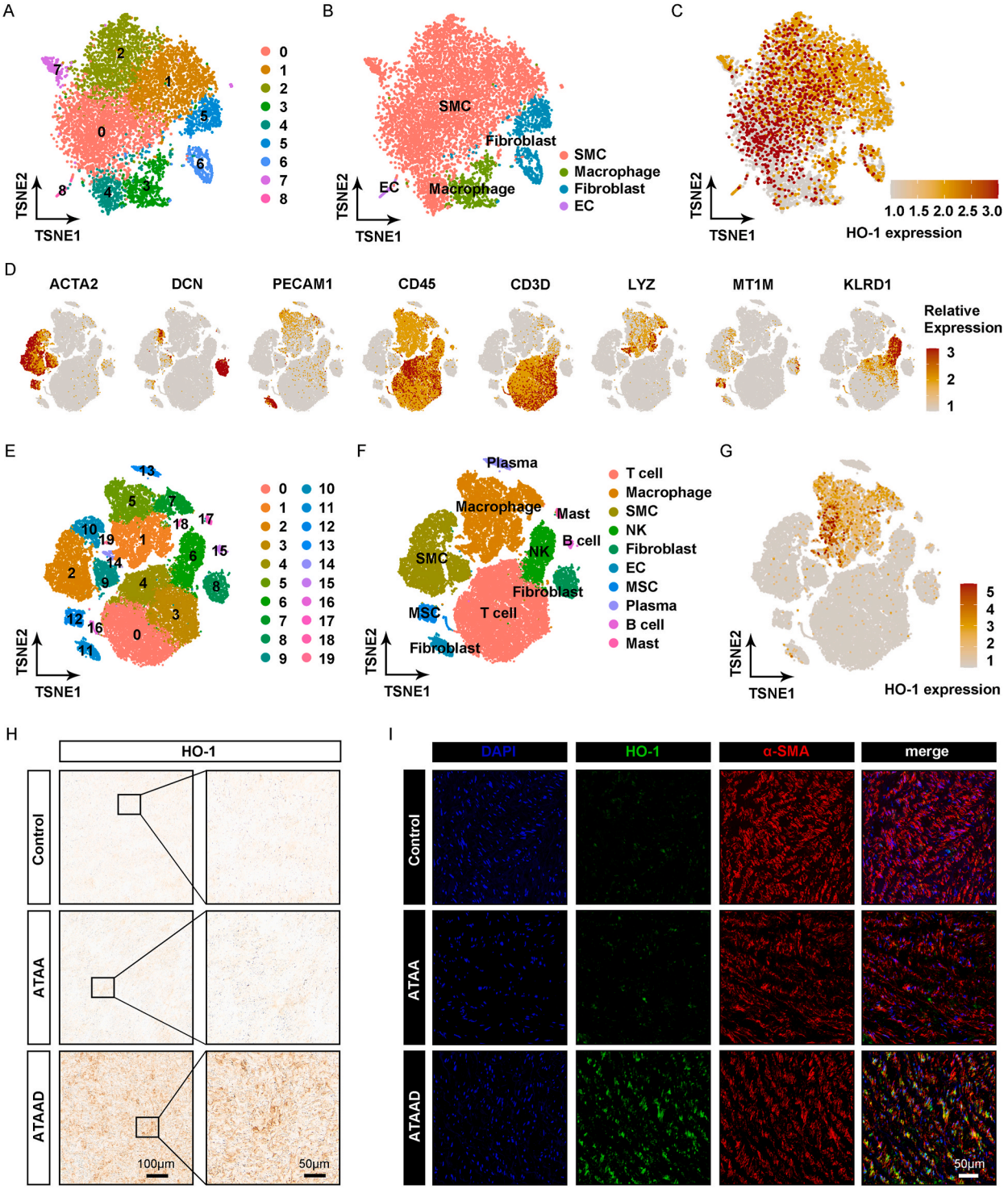

Fig. 4. HO-1 is Upregulated in VSMC of ATAAD Aorta. **(A)** TSNE plots of different cell clusters in ATAAD. **(B)** TSNE plots of different cell types in ATAAD. **(C)** TSNE plots of HO-1 expression in ATAAD. **(D)** Conserved cell markers in human control and aneurysmal thoracic aortic tissues. **(E)** TSNE plots of different cell clusters in control and ATAA. **(F)** TSNE plots of different cell types in control and ATAA. **(G)** TSNE plots of HO-1 expression in control and ATAA. **(H)** IHC staining of HO-1 in control, ATAA and ATAAD specimens. **(I)** IF staining of HO-1/α-SMA in control, ATAA and ATAAD specimens. n = 5 per group. IHC, Immunohistochemistry; IF, Immunofluorescence.

3.2. HO-1 is a key signature of ferroptosis in ATAAD

Above bioinformatic findings were further confirmed by experimental validation. Prussian blue staining showed significant iron accumulation in the ATAAD tissues marked by blue area (Fig. 2A-B). Lipid peroxidation assay showed the concentration of MDA, representative product of lipid peroxidation, was significantly increased in ATAAD (Fig. 2C). IHC staining further demonstrated that 4-HNE, a marker of lipid peroxidation, was significantly overexpressed in ATAAD. GPX-4, the key enzyme of GSH-GSSG antioxidant system, was significantly downregulated (Fig. 2D-E). These results verified that ferroptosis was a critical manner of RCD in ATAAD.

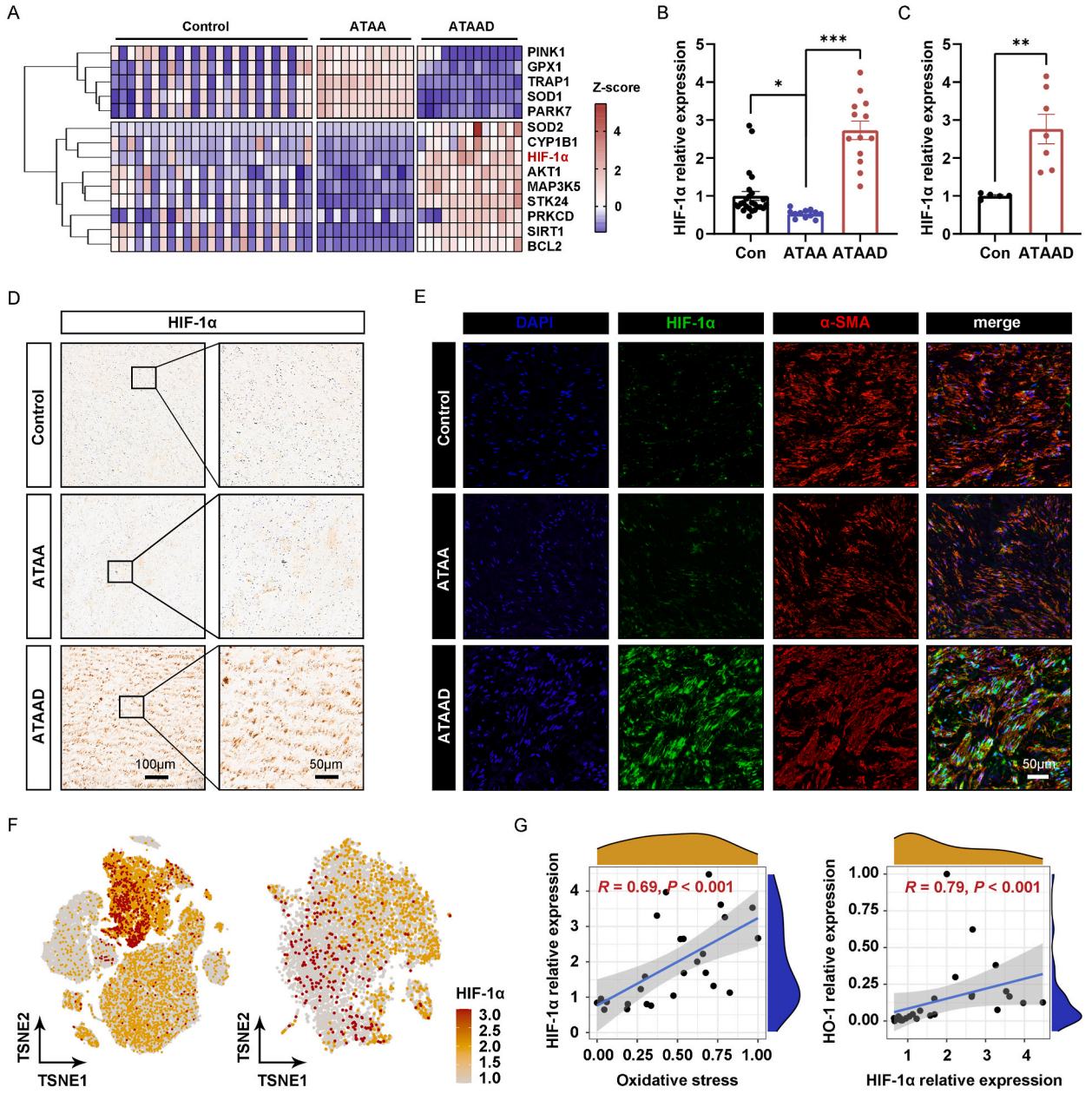

Fig. 5. HIF-1α is Overexpressed in VSMC of ATAAD and Closely Correlated with HO-1 Expression. **(A)** Heatmap of differentially expressed oxidative stress related genes in ATAAD. **(B)** Expression of HIF-1α in control, ATAA and ATAAD specimens. **(C)** Confirmation of HIF-1α expression in GSE52093. **(D)** IHC staining of HIF-1α in control, ATAA and ATAAD specimens. **(E)** IF staining of HIF-1α/α-SMA in control, ATAA and ATAAD specimens. n = 5 per group. **(F)** TSNE plots of HIF-1α expression in control and ATAA specimens (left). TSNE plots of HIF-1α expression in ATAAD specimen (right). **(G)** Correlation analysis between oxidative stress and HIF-1α relative expression (left). Correlation analysis between HIF-1α and HO-1 relative expression (right). Data shown are means ± SEM. Statistical analysis was performed through one-way ANOVA combined with Bonferroni correction (Panel B) and Student's two-tailed *t*-test with Welch's correction (Panel C). $^{*}P < 0.05$, $^{**}P < 0.01$, $^{***}P < 0.001$.

Furthermore, it is valuable to identify which molecule may play a key role in the ferroptosis of ATAAD. First, differential analysis was performed between control and ATAAD ascending aorta. A total of 1977 DEGs was identified in the test group GSE153434 and GSE107844 including 9 FRGs ($|logFC| > 1$ and P value < 0.05). Differently expressed FRGs were shown as PPI network in Fig. 2F. Heatmap of differentially expressed FRGs revealed overexpression of LPCAT3, SLC7A11, STEAP3, MT1G, HO-1, AKR1C3, FTH1 and SAT1 while DPP4 was downregulated in ATAAD compared with control specimens (Fig. 2G). These 9 FRGs were further used for identification of key signature in ATAAD through machine learning algorithms. First, random forest was used for selection. We set one as the cut-off value of MeanDecreaseGini and identified HO-1, SAT1, MT1G and LPCAT3 as hub FRGs in ATAAD. Specifically, MeanDecreaseGini of HO-1 was obviously higher than other three hub FRGs (Fig. 2H). Further, SVM-RFE screened HO-1 and DPP4 as hub FRGs in ATAAD (Fig. 2I). Through integration and intersection, HO-1 was finally confirmed as a key signature in ATAAD (Fig. 2J). This result was in line with the fact that HO-1 was the only intersection gene among DEGs of three GEO datasets and FRGs (Fig. 2K). Fold change of HO-1 in ATAAD compared with control specimens in three datasets were 7.84, 13.08 and 9.08, respectively (Fig. 2L). Our results demonstrated that HO-1 may be a key signature of ferroptosis in ATAAD.

3.3. Oxidative stress is associated with ferroptosis and HO-1 expression in ATAAD

To better understand the potential mechanism of increased HO-1 expression in ATAAD, we checked whether ferroptosis and HO-1 were also upregulated in non-dissected ATAA that shares similar histopathologic features with ATAAD. We obtained 12 control and 12 ATAA specimens from GSE140947 (Fig. 3A). Surprisingly, GSEA found no significant enrichment of six manners of RCD in ATAA (Fig. 3B). Further ssGSEA only revealed that autophagy was significantly downregulated in ATAA compared with control ascending aorta (Fig. 3C). Comparison of HO-1 expression revealed that HO-1 was not significantly altered in ATAA compared with control samples, along with no change of several FRGs including FTH1 and SLC7A11 (Fig. 3D).

Considering that ferroptosis and HO-1 were upregulated in ATAAD but not ATAA, it is valuable to explore the difference between ATAAD and ATAA on molecular levels. GO analysis demonstrated that oxidative stress was significantly upregulated in ATAAD compared with ATAA (**Supplementary File 4**). Oxidative stress related pathways were significantly activated in ATAAD such as MAPK cascade, JNK cascade and intrinsic apoptotic signaling pathway in response to oxidative stress (Fig. 3E). Next, we retrieved 396 genes from significantly enriched oxidative stress related pathways (**Supplementary File 4**). Oxidative stress was evaluated based on the expression of these genes through ssGSEA. Correlation analysis revealed that oxidative stress was positively correlated with ferroptosis (Fig. 3F, $R = 0.80$, $P < 0.001$) and HO-1 relative expression (Fig. 3G, $R = 0.82$, $P < 0.001$). Therefore, we hypothesized that upregulation of ferroptosis and HO-1 expression might be closely associated with high-level oxidative stress in ATAAD.

3.4. HO-1 is mainly overexpressed in the VSMC and macrophage of ATAAD

Since transcriptomic analysis suggested overexpression of HO-1 in ATAAD, we performed further investigations on cellular expression of HO-1. We performed single-nucleus extraction, 10X genomics sequencing and obtained a total of 5,680 aortic cells from ATAAD specimen (Fig. 4A). According to conserved cell markers, 9 clusters and 4 cell types were identified including VSMC, fibroblast, macrophage, and endothelial cell (EC) (Fig. 4B). Analysis of HO-1 expression demonstrated that HO-1 was highly expressed in VSMC, which is the main cell type in the aortic walls (Fig. 4C). In addition, HO-1 is also expressed in macrophage and fibroblast. The cell quantity of EC is too low for analysis. Single-cell transcriptomic analysis of GSE155468 demonstrated that HO-1 was highly expressed in macrophage but lowly expressed in other cell types of control and ATAA aorta (Fig. 4D–G). Therefore, VSMC and macrophage were mainly focused for further investigation on the cellular expression of HO-1.

Histological staining of control, ATAA and ATAAD were further performed to confirm cellular expression of HO-1. IHC staining revealed that HO-1 was lowly expressed in control and ATAA specimens. However, it was highly expressed within ATAAD aortic tissue (Fig. 4H). Further, IF staining confirmed that HO-1 was co-localized with+VSMC marked by α-SMA in ATAAD specimens (Fig. 4I). In addition, IHC staining of CD68 revealed accumulation of macrophages within thoracic aorta of ATAAD (Supplementary Fig. 1A). Dual IF staining showed that HO-1 was also expressed in the macrophages (Supplementary Fig. 1B). Taken together, these results suggested that VSMC and macrophage could provide the expression of HO-1 in ATAAD.

3.5. HIF-1α is overexpressed and closely correlated with HO-1 expression in the VSMC of ATAAD

Considering that VSMC is a major cell type within thoracic aortic walls and the overexpression of HO-1 was obviously observed in VSMC of ATAAD, we next mainly focused on the underlying mechanisms. Since ferroptosis and HO-1 expression were closely associated with high condition of oxidative stress, we hypothesized that HO-1 might be induced under oxidative stress in VSMC of ATAAD. Hypoxia induced factor 1α (HIF-1α) was a classical molecular to be induced by oxidative stress and was among differentially expressed oxidative stress related genes (Fig. 5A). HIF-1α was significantly overexpressed in ATAAD compared with control and ATAA (Fig. 5B–C). Thus, HIF-1α was screened as a key participator of oxidative stress in ATAAD.

IHC and IF staining confirmed these findings (Fig. 5D–E). Specifically, co-staining of HIF-1α with α-SMA revealed upregulation of HIF-1α in VSMC. Similarly, single-cell/nucleus transcriptomic analysis demonstrated that HIF-1α was lowly expressed in VSMC of thoracic aorta in control and ATAA but was relatively highly expressed in VSMC of ATAAD specimens (Fig. 5F). Next, we speculated that oxidative stress might induce expression of HO-1 through HIF-1α. Correlation analysis showed that HIF-1α expression was positively correlated with oxidative stress (Fig. 5G, $R = 0.69$, $P < 0.001$) and HO-1 expression (Fig. 5G, $R = 0.79$, $P < 0.001$). Collectively, these bioinformatic analyses suggested a potential regulatory relationship between oxidative stress, HIF-1α and HO-1

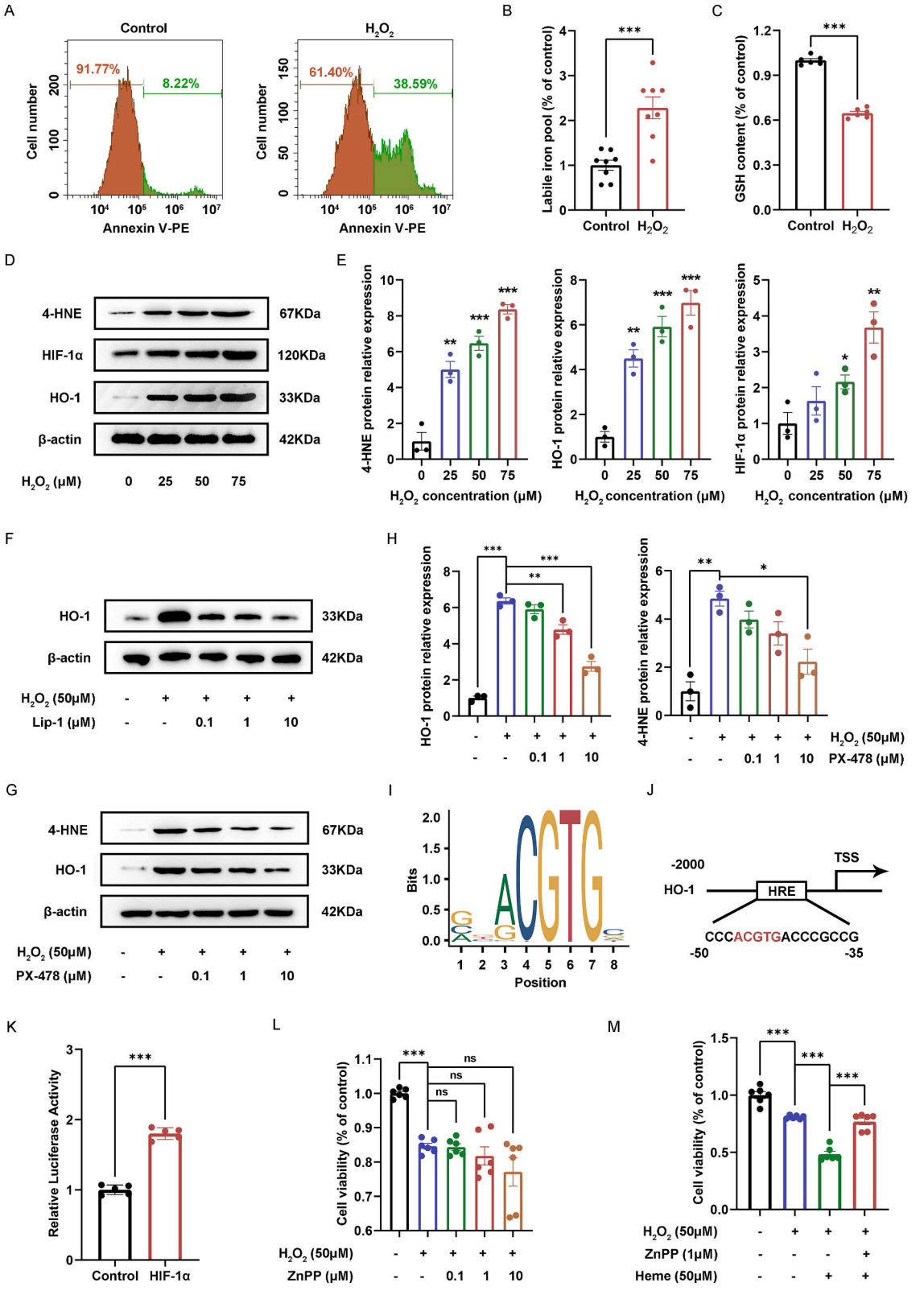

(caption on next page)

Fig. 6. HIF-1α/HO-1 mediated ferroptosis is involved in oxidative stress induced HA-VSMC damage. (A) Annexin V/7-AAD assay. **(B)** Labile iron pool analysis. **(C)** GSH assay. **(D)** Western blot of HO-1, HIF-1α and 4-HNE in HA-VSMC with three concentrations of H_2O_2 (25, 50 and 75 μM). **(E)** Statistical analysis of Western blot. **(F)** Western blot assay of HO-1 in HA-VSMC co-incubated with 50 μM H_2O_2 and different concentrations of ferroptosis inhibitor Lip-1 (0.1, 1, 10 μM). **(G)** Western blot assay of HO-1 and 4-HNE in HA-VSMC co-incubated with 50 μM H_2O_2 and different concentrations of HIF-1α inhibitor PX-478 (0.1, 1, 10 μM). **(H)** Statistical analysis of Western blot. **(I)** HIF-1α binding sequence HRE. **(J)** The predicted sequence of HIF-1α binding sites in the promoter region of HO-1 (2000 bases forward TSS, −2000/0) on the basis of JASPAR database. HRE, −49/-40. **(K)** Luciferase reporter gene assay to test whether HIF-1α binds to promoter region of HO-1. **(L)** Cell viability of HA-VSMC co-treated with H_2O_2 and HO-1 inhibitor ZnPP. **(M)** Cell viability of HA-VSMC co-treated with H_2O_2, heme and HO-1 inhibitor ZnPP. H_2O_2, hydrogen peroxide; GSH, glutathione; Lip-1, liproxstatin-1; HRE, hypoxia response element; TSS, transcription starting site; ZnPP, zinc protoporphyrin. MTT assay, n = 6 per group. Western blot, n = 3 per group. Data shown are means ± SEM. Statistical analysis between two groups was performed through Student's two-tailed *t*-test (Panel B, C and G). Statistical analysis between multiple groups was performed through one-way ANOVA combined with Bonferroni correction (Panel E, H, L, and M). Uncropped and non-adjusted images of Western blot assay were available in **Supplementary File 5**. $^{*}P < 0.05$, $^{**}P < 0.01$, $^{***}P < 0.001$, ns = not significant.

expression.

3.6. HIF-1α/HO-1 mediated ferroptosis is involved in oxidative stress induced HA-VSMC damage

To verify the oxidative stress/HIF-1α/HO-1 axis in VSMC ferroptosis, in vitro experiment in HA-VSMC cell line was performed. First, we focused on whether ferroptosis was involved in oxidative stress induced VSMC damage. H_2O_2 was used to establish the in vitro model of oxidative stress in HA-VSMC [40]. In our results, H_2O_2 dose-dependently inhibited cell viability of HA-VSMC via MTT assay (Supplementary Fig. 2, IC50 = 64.21 μM). Annexin V/7-AAD assay provided evidence that 50 μM H_2O_2 induced cell damage and death of HA-VSMC (Fig. 6A). Labile iron pool analysis suggested iron overload and GSH assay showed significantly lower cellular concentration of GSH in this condition (Fig. 6B–C). Further, three concentrations (25, 50 and 75 μM) was used to reveal that H_2O_2 could dose-dependently induce expression of lipid peroxidation marker 4-HNE (Fig. 6D–E). These results consolidated that ferroptosis was involved in H_2O_2 induced VSMC damage.

We further verified whether H_2O_2 induced VSMC ferroptosis via HO-1. Western blot assay clearly showed that H_2O_2 induced the overexpression of HO-1 by 4.50, 5.92 and 6.98-fold at the concentration of 25, 50 and 75 μM, respectively, which matched the fold change of HO-1 in clinical ATAAD specimens. Ferroptosis inhibitor Lip-1 remarkably suppressed the expression of HO-1 induced by H_2O_2 in a dose-dependent manner (Fig. 6F). These results underlined the important role of HO-1 mediated ferroptosis in H_2O_2 induced VSMC damage.

We next tested whether oxidative stress could induce the expression of HO-1 and further ferroptosis through HIF-1α. Western blot assay suggested overexpression of HIF-1α in HA-VSMC with treatment of H_2O_2 (Fig. 6D). Co-incubation with PX-478, a HIF-1α inhibitor, could dose-dependently suppress ferroptosis marked by decrease of 4-HNE. In addition, PX-478 inhibited the overexpression of HO-1 induced by H_2O_2 (Fig. 6G–H). This result further provided evidence that HIF-1α/HO-1 axis could participate in oxidative stress induced VSMC ferroptosis. We further specify the molecular regulation between HIF-1α and HO-1. Considering that HIF-1α is a transcriptional factor, we hypothesized that HIF-1α might direct initiate the transcription of HO-1. One predicted sequence of HRE was found on the promoter region of HO-1 (Fig. 6I–J). Then, we performed luciferase reporter gene assay to detect whether HIF-1α could bind to the promotor region of HO-1. As expected, HIF-1α overexpression increased the luciferase activity after HO-1 promoter sequence, which supported that HIF-1α could transcriptionally regulate the expression of HO-1 (Fig. 6K).

We finally explored whether inhibition of HO-1 could alleviate VSMC damage induced by oxidative stress. Interestingly, HO-1 inhibitor ZnPP did not attenuate H_2O_2-induced cell damage of HA-VSMC (Fig. 6L). This result indicated that ZnPP did not directly reduce VSMC damage induced by oxidative stress, which might be attributed to the difference between the microenvironment of oxidative stress in vitro and in ATAAD tissues. The microenvironment of ATAAD is not only characterized by activated oxidative stress, but also contains large number of erythrocytes with heme. To better simulate the microenvironment in ATAAD tissues, heme was added into the cell medium and co-incubated with H_2O_2. When heme was added into the medium, H_2O_2-induced HA-VSMC damage was worsened. ZnPP administration significantly protected H_2O_2-induced HA-VSMC damage when co-incubated with heme (Fig. 6M).

4. Discussion

With blood flow into the false lumen of ATAAD, oxidative stress drives large expression of HO-1 through HIF-1α in VSMC. Infiltrated macrophages also express and offer HO-1 as well. HO-1 degrades heme, which produces large amount of free iron and lead to ferroptosis of VSMC. With VSMC death, HO-1 might be released into microenvironment of false lumen and produce new cycles of iron overload and ferroptosis. Positive feedback of oxidative stress, HO-1 expression and ferroptosis might lead to false lumen enlargement and dissection progression (**Graphic Abstract**).

Ferroptosis was identified as a critical manner of RCD based on bioinformatic methods in ATAAD, which is an iron-dependent RCD. Iron is distributed in hemoglobin, myoglobin, and iron-dependent enzymes as functional iron, stored in liver and spleen for medullary hematopoiesis and excreted from dejection, urine, skin, and milk [41]. Iron plays a key role in cell longevity and is involved in a wide range of biological processes including oxygen storage and transportation, DNA repair, mitochondrial respiration, and others. However, excessive iron has detrimental and toxic effects on cell biology termed as ferroptosis. Iron is mainly originated from daily food intake as well as heme degradation [41]. When erythrocytes are destroyed, the hemoglobin is released and degraded into globin and

heme. Heme is further degraded by heme oxygenase to produce iron. The interaction of iron with oxygen or hydrogen peroxide leads to production of reactive oxygen species and further lipid peroxidation [42]. Notably, the false lumen of ATAAD contains large number of erythrocytes to produce excessive iron for ferroptosis. This may explain why ferroptosis is statistically most significant among six RCDs in ATAAD.

Since ferroptosis might serve as a critical manner of RCD in ATAAD, we further identified HO-1 as a prominent hallmark gene of ferroptosis on clinical tissue levels. HO is mainly classified into two categories including HO-1 and HO-2. HO-2 is constitutively expressed while HO-1 might be induced under certain circumstances [43]. Both transcriptome datasets and histological staining confirmed significant elevation of HO-1 in ATAAD specimens. For further investigation of its biological functions, it is valuable to specify cellular expression of HO-1. Our data suggested that VSMC is an important source of HO-1 in ATAAD, which is the major cell type within thoracic aortic walls [44]. Although HO-1 was also expressed in infiltrated aortic macrophage, the quantity of macrophage might not be as many as VSMC in the media layer. Consistently, our morphological staining has demonstrated that HO-1 was highly expressed and mainly co-localized with VSMC. Therefore, we speculated that the overexpression of HO-1 in VSMC is more likely to play the dominant role in the VSMC ferroptosis in ATAAD. In vitro experiments verified that classical ferroptosis inhibitor liproxstatin-1 could suppress the expression of HO-1 in H_2O_2-induced ferroptosis model. Our findings were in line with previous in vitro experiments, which demonstrated that HO-1 was overexpressed in both cystine deprivation and imidazole ketone erastin induced VSMC ferroptosis models [45].

However, it remains unknown whether ferroptosis and HO-1 overexpression are a cause or effect of ATAAD. It has been reported that serum and aortic iron were increased in ATAAD [46]. Consistently, previous studies observed upregulation of ferroptosis in ATAAD marked by overexpression of several FRGs including SLC7A11 and FSP1 and the downregulation of GPX4 [47,48]. In addition, targeting at ferroptosis might have the potential value in the alleviation of aortic dissection [47,49]. These studies supported that ferroptosis might participate in the pathogenesis of aortic dissection. As we know, aortic specimens were isolated from open surgery of ATAAD patients after dissection onset, which have already been exposed to a microenvironment of high stress and inflammatory response. In our opinion, it is difficult to clarify whether ferroptosis occurs before or after ATAAD onset [50]. Interestingly, ferroptosis and HO-1 was not upregulated in ATAA specimens. Thus, HO-1 mediated ferroptosis may be induced after dissection onset.

Special microenvironment within false lumen might create optimal conditions for ferroptosis. It has been well acknowledged that ferroptosis could be induced by oxidative stress and thus form positive feedback to drive inflammation and immune response [51,52]. Dissection onset and intimal tearing are a great stress for human body, especially oxidative stress. Exposure to hemoglobin and immune cells may drive severe oxidative stress and VSMC damage within false lumen. In line with these, our results also demonstrated that ferroptosis was closely associated with reactive oxygen species and oxidative stress. To find out downstream molecular mechanisms of HO-1 overexpression, we compared ATAAD and ATAA to screen key oxidative stress related genes. Specifically, we identified HIF-1α as a critical transcriptional regulator of HO-1 in HA-VSMC. Over the decades, HIF-1α has been proved to be induced under hypoxia, oxidative stress and other transient stimulus [53]. Although its overexpression has already been identified in several literatures on ATAAD [45,54,55], molecular mechanisms of how HIF-1α promotes dissection progression remain still little known. Here, we have demonstrated a novel mechanism of VSMC ferroptosis through HIF-1α/HO-1 axis in response to oxidative stress.

In vitro experiments of this study are linked with our findings in ATAAD tissues. First, ATAAD is characterized by a microenvironment of oxidative stress. In vitro experiments simulated this condition in HA-VSMC by H_2O_2 stimulation. Next, oxidative stress and ferroptosis are associated with the overexpression of HIF-1α/HO-1 in ATAAD tissues. In line with this finding, HIF-1α/HO-1/ferroptosis axis was confirmed in vitro through H_2O_2 induced HA-VSMC model. In addition, ATAAD tissues are exposed to large amount of heme, which could be degraded by HO-1 into free iron. In the absence of heme, HO-1 inhibitor ZnPP had little effect on VSMC survival with H_2O_2. However, protective effect of ZnPP was observed when heme was co-incubated. This finding emphasized the importance of HIF-1α/HO-1 mediated ferroptosis in the microenvironment of oxidative stress with heme, which is closer to ATAAD tissues in vivo. Therefore, we hypothesized that HIF-1α/HO-1 mediated VSMC ferroptosis might play a key role in the VSMC damage during dissection progression.

This study has some limitations. In this study, we put out a reasonable hypothesis of ferroptosis and dissection progression based on current bioinformatic analysis and in vitro experiments. Protective effect of HO-1 inhibitor ZnPP was only investigated on HA-VSMC in vitro. Further in vivo experiments are warranted to further extrapolate these findings in ATAAD tissues. However, it is difficult to simulate false lumen progression and dissection progression in vivo. Existing mouse model only simulate a pattern of aortic dilation and has different mechanisms from human ATAAD. In addition, we cannot totally exclude other manners of cell death from our in vitro experiments. Comprehensive understanding of VSMC damage in ATAAD is warranted in the future.

5. Conclusions

HO-1 is a key signature of VSMC ferroptosis in ATAAD. HIF-1α/HO-1 mediated ferroptosis might participate in oxidative stress induced VSMC damage. HO-1 mediated ferroptosis might serve as a novel therapeutic target to control dissection progression in the future.

Ethics approval and consent to participate

Study protocols involving clinical specimens from patients were reviewed and approved by Ethical Committee of Zhongshan Hospital, Fudan University (Ethical number: B2022-374R). Written informed consent for experimentation was obtained from all patients.

Consent for publication

Yes.

Funding statement

This work was sponsored by the National Natural Science Foundation of China (No. 82200526), the Shanghai Rising-Star Program (No. 23QB1400900), the Shanghai "Rising Stars of Medical Talents" Youth Development Program (No. SHWRS2023-62), and the Clinical Research Fund of Shanghai Municipal Health Commission (No. 20224Y0286).

CRediT authorship contribution statement

Wenyu Song: Writing - original draft, Methodology, Investigation, Formal analysis. **Yifu Chen:** Writing - original draft, Methodology, Investigation, Formal analysis. **Lieyang Qin:** Writing - original draft, Methodology, Investigation, Formal analysis. **Xinyuan Xu:** Writing - original draft, Investigation, Formal analysis. **Yu Sun:** Writing - original draft, Methodology, Formal analysis. **Mingzhu Zhong:** Writing - original draft, Investigation, Formal analysis. **Yuntao Lu:** Writing - original draft, Investigation, Formal analysis. **Kui Hu:** Writing - review & editing, Resources, Investigation. **Lai Wei:** Writing - review & editing, Supervision, Conceptualization. **Jinmiao Chen:** Writing - review & editing, Writing - original draft, Supervision, Resources, Conceptualization.

Declaration of competing interest

The authors declare that they have no known competing financial interests or personal relationships that could have appeared to influence the work reported in this paper.

Acknowledgements

Vectorial elements of the figures were obtained from SERVIER Medical Art (https://smart.servier.com/) under a Creative Common Attribution 3.0 Generic License (https://creativecommons.org/licenses/by/3.0/).

Appendix A. Supplementary data

Supplementary data to this article can be found online at https://doi.org/10.1016/j.heliyon.2023.e22857.

References

[1] E.M. Isselbacher, O. Preventza, J.H. Black 3rd, J.G. Augoustides, A.W. Beck, M.A. Bolen, A.C. Braverman, B.E. Bray, M.M. Brown-Zimmerman, E.P. Chen, T. J. Collins, A. DeAnda Jr., C.L. Fanola, L.N. Girardi, C.W. Hicks, D.S. Hui, W.S. Jones, V. Kalahasti, K.M. Kim, D.M. Milewicz, G.S. Oderich, L. Ogbechie, S. B. Promes, E.G. Ross, M.L. Schermerhorn, S.S. Times, E.E. Tseng, G.J. Wang, Y.J. Woo, 2022 ACC/AHA guideline for the diagnosis and management of aortic disease: a report of the American heart association/American college of cardiology joint committee on clinical practice guidelines, Circulation (2022), https://doi.org/10.1161/CIR.0000000000001106.

[2] E.M. Isselbacher, Thoracic and abdominal aortic aneurysms, Circulation 111 (2005) 816–828, https://doi.org/10.1161/01.CIR.0000154569.08857.7A.

[3] E.M. Isselbacher, O. Preventza, J. Hamilton Black 3rd, J.G. Augoustides, A.W. Beck, M.A. Bolen, A.C. Braverman, B.E. Bray, M.M. Brown-Zimmerman, E.P. Chen, T.J. Collins, A. DeAnda Jr., C.L. Fanola, L.N. Girardi, C.W. Hicks, D.S. Hui, W. Schuyler Jones, V. Kalahasti, K.M. Kim, D.M. Milewicz, G.S. Oderich, L. Ogbechie, S.B. Promes, E. Gyang Ross, M.L. Schermerhorn, S. Singleton Times, E.E. Tseng, G.J. Wang, Y.J. Woo, 2022 ACC/AHA guideline for the diagnosis and management of aortic disease: a report of the American heart association/American college of cardiology joint committee on clinical practice guidelines, Circulation 146 (2022) e334–e482, https://doi.org/10.1161/CIR.0000000000001106.

[4] K.M. Harris, C.A. Nienaber, M.D. Peterson, E.M. Woznicki, A.C. Braverman, S. Trimarchi, T. Myrmel, R. Pyeritz, S. Hutchison, C. Strauss, M.P. Ehrlich, T. G. Gleason, A. Korach, D.G. Montgomery, E.M. Isselbacher, K.A. Eagle, Early mortality in type A acute aortic dissection: insights from the international registry of acute aortic dissection, JAMA Cardiol 7 (2022) 1009–1015, https://doi.org/10.1001/jamacardio.2022.2718.

[5] D. Li, L. Ye, Y. He, X. Cao, J. Liu, W. Zhong, L. Cao, R. Zeng, Z. Zeng, Z. Wan, Y. Cao, False lumen status in patients with acute aortic dissection: a systematic review and meta-analysis, J. Am. Heart Assoc. 5 (2016), https://doi.org/10.1161/JAHA.115.003172.

[6] D. Tang, R. Kang, T.V. Berghe, P. Vandenabeele, G. Kroemer, The molecular machinery of regulated cell death, Cell Res. 29 (2019) 347–364, https://doi.org/10.1038/s41422-019-0164-5.

[7] X. Chen, J. Li, R. Kang, D.J. Klionsky, D. Tang, Ferroptosis: machinery and regulation, Autophagy 17 (2021) 2054–2081, https://doi.org/10.1080/15548627.2020.1810918.

[8] N. Imuta, O. Hori, Y. Kitao, Y. Tabata, T. Yoshimoto, T. Matsuyama, S. Ogawa, Hypoxia-mediated induction of heme oxygenase type I and carbon monoxide release from astrocytes protects nearby cerebral neurons from hypoxia-mediated apoptosis, Antioxidants Redox Signal. 9 (2007) 543–552, https://doi.org/10.1089/ars.2006.1519.

[9] D.D. Haines, A. Tosaki, Role of heme oxygenases in cardiovascular syndromes and Co-morbidities, Curr. Pharmaceut. Des. 24 (2018) 2322–2325, https://doi.org/10.2174/1381612824666180727110353.

[10] W. Song, F. Lu, Z. Ding, L. Huang, K. Hu, J. Chen, L. Wei, Identification of heparan sulfate in dilated cardiomyopathy by integrated bioinformatics analysis, Front Cardiovasc Med 9 (2022), 900428, https://doi.org/10.3389/fcvm.2022.900428.

[11] J. Costa-Silva, D. Domingues, F.M. Lopes, RNA-Seq differential expression analysis: an extended review and a software tool, PLoS One 12 (2017), e0190152, https://doi.org/10.1371/journal.pone.0190152.

[12] H.M. Wu, Y.J. Tien, M.R. Ho, H.G. Hwu, W.C. Lin, M.H. Tao, C.H. Chen, Covariate-adjusted heatmaps for visualizing biological data via correlation decomposition, Bioinformatics 34 (2018) 3529–3538, https://doi.org/10.1093/bioinformatics/bty335.

[13] C. von Mering, M. Huynen, D. Jaeggi, S. Schmidt, P. Bork, B. Snel, STRING: a database of predicted functional associations between proteins, Nucleic Acids Res. 31 (2003) 258–261, https://doi.org/10.1093/nar/gkg034.

[14] P. Shannon, A. Markiel, O. Ozier, N.S. Baliga, J.T. Wang, D. Ramage, N. Amin, B. Schwikowski, T. Ideker, Cytoscape: a software environment for integrated models of biomolecular interaction networks, Genome Res. 13 (2003) 2498–2504, https://doi.org/10.1101/gr.1239303.

[15] C. The, Gene ontology, the gene ontology resource: 20 years and still GOing strong, Nucleic Acids Res. 47 (2019) D330–D338, https://doi.org/10.1093/nar/gky1055.

[16] B. Levine, G. Kroemer, Biological functions of autophagy genes: a disease perspective, Cell 176 (2019) 11–42, https://doi.org/10.1016/j.cell.2018.09.048.

[17] D. Tang, X. Chen, G. Kroemer, Cuproptosis: a copper-triggered modality of mitochondrial cell death, Cell Res. 32 (2022) 417–418, https://doi.org/10.1038/s41422-022-00653-7.

[18] G. Kroemer, L. Galluzzi, O. Kepp, L. Zitvogel, Immunogenic cell death in cancer therapy, Annu. Rev. Immunol. 31 (2013) 51–72, https://doi.org/10.1146/annurev-immunol-032712-100008.

[19] L. Galluzzi, O. Kepp, F.K. Chan, G. Kroemer, Necroptosis: mechanisms and relevance to disease, Annu. Rev. Pathol. 12 (2017) 103–130, https://doi.org/10.1146/annurev-pathol-052016-100247.

[20] P. Yu, X. Zhang, N. Liu, L. Tang, C. Peng, X. Chen, Pyroptosis: mechanisms and diseases, Signal Transduct. Targeted Ther. 6 (2021) 128, https://doi.org/10.1038/s41392-021-00507-5.

[21] A. Subramanian, P. Tamayo, V.K. Mootha, S. Mukherjee, B.L. Ebert, M.A. Gillette, A. Paulovich, S.L. Pomeroy, T.R. Golub, E.S. Lander, J.P. Mesirov, Gene set enrichment analysis: a knowledge-based approach for interpreting genome-wide expression profiles, Proc. Natl. Acad. Sci. U.S.A. 102 (2005) 15545–15550, https://doi.org/10.1073/pnas.0506580102.

[22] T.U. Islam, Min-max approach for comparison of univariate normality tests, PLoS One 16 (2021), e0255024, https://doi.org/10.1371/journal.pone.0255024.

[23] S. Hanzelmann, R. Castelo, J. Guinney, GSVA: gene set variation analysis for microarray and RNA-seq data, BMC Bioinf. 14 (2013) 7, https://doi.org/10.1186/1471-2105-14-7.

[24] A. Cutler, J.R. Stevens, Random forests for microarrays, Methods Enzymol. 411 (2006) 422–432, https://doi.org/10.1016/S0076-6879(06)11023-X.

[25] X. Lin, F. Yang, L. Zhou, P. Yin, H. Kong, W. Xing, X. Lu, L. Jia, Q. Wang, G. Xu, A support vector machine-recursive feature elimination feature selection method based on artificial contrast variables and mutual information, J. Chromatogr., B: Anal. Technol. Biomed. Life Sci. 910 (2012) 149–155, https://doi.org/10.1016/j.jchromb.2012.05.020.

[26] Y. Li, P. Ren, A. Dawson, H.G. Vasquez, W. Ageedi, C. Zhang, W. Luo, R. Chen, Y. Li, S. Kim, H.S. Lu, L.A. Cassis, J.S. Coselli, A. Daugherty, Y.H. Shen, S. A. LeMaire, Single-cell transcriptome analysis reveals dynamic cell populations and differential gene expression patterns in control and aneurysmal human aortic tissue, Circulation 142 (2020) 1374–1388, https://doi.org/10.1161/CIRCULATIONAHA.120.046528.

[27] D. Grun, A. van Oudenaarden, Design and analysis of single-cell sequencing experiments, Cell 163 (2015) 799–810, https://doi.org/10.1016/j.cell.2015.10.039.

[28] W. Song, L. Qin, Y. Chen, J. Chen, L. Wei, Single-cell transcriptome analysis identifies Versican(+) myofibroblast as a hallmark for thoracic aortic aneurysm marked by activation of PI3K-AKT signaling pathway, Biochem. Biophys. Res. Commun. 643 (2023) 175–185, https://doi.org/10.1016/j.bbrc.2022.12.086.

[29] W.H. Park, Upregulated thioredoxin and its reductase prevent H(2)O(2)-induced growth inhibition and death in human pulmonary artery smooth muscle cells, Toxicol. Vitro 61 (2019), 104590, https://doi.org/10.1016/j.tiv.2019.104590.

[30] L. Han, Y. Zhang, B. Zhao, J. Yue, Z. Chen, G. Lei, C. Huang, W. Chen, MicroRNA 101 attenuated NSCLC proliferation through IDH2/HIFalpha Axis suppression in the warburg effect, Oxid. Med. Cell. Longev. 2022 (2022), 4938811, https://doi.org/10.1155/2022/4938811.

[31] L. Sun, Y. Zhang, S. Wen, Q. Li, R. Chen, X. Lai, Z. Zhang, Z. Zhou, Y. Xie, X. Zheng, K. Zhang, D. Li, S. Sun, Extract of Jasminum grandiflorum L. alleviates CCl (4)-induced liver injury by decreasing inflammation, oxidative stress and hepatic CYP2E1 expression in mice, Biomed. Pharmacother. 152 (2022), 113255, https://doi.org/10.1016/j.biopha.2022.113255.

[32] C. Bao, C. Liu, Q. Liu, L. Hua, J. Hu, Z. Li, S. Xu, Liproxstatin-1 alleviates LPS/IL-13-induced bronchial epithelial cell injury and neutrophilic asthma in mice by inhibiting ferroptosis, Int. Immunopharm. 109 (2022), 108770, https://doi.org/10.1016/j.intimp.2022.108770.

[33] N. Bhaskaran, S. Shukla, R. Kanwal, J.K. Srivastava, S. Gupta, Induction of heme oxygenase-1 by chamomile protects murine macrophages against oxidative stress, Life Sci. 90 (2012) 1027–1033, https://doi.org/10.1016/j.lfs.2012.05.019.

[34] N.R. Chintagari, J. Nguyen, J.D. Belcher, G.M. Vercellotti, A.I. Alayash, Haptoglobin attenuates hemoglobin-induced heme oxygenase-1 in renal proximal tubule cells and kidneys of a mouse model of sickle cell disease, Blood Cells Mol. Dis. 54 (2015) 302–306, https://doi.org/10.1016/j.bcmd.2014.12.001.

[35] W.Y. Song, X.H. Jiang, Y. Ding, Y. Wang, M.X. Zhou, Y. Xia, C.Y. Zhang, C.C. Yin, C. Qiu, K. Li, P. Sun, X. Han, Inhibition of heparanase protects against pancreatic beta cell death in streptozotocin-induced diabetic mice via reducing intra-islet inflammatory cell infiltration, Br. J. Pharmacol. 177 (2020) 4433–4447, https://doi.org/10.1111/bph.15183.

[36] B.R. Stockwell, J.P. Friedmann Angeli, H. Bayir, A.I. Bush, M. Conrad, S.J. Dixon, S. Fulda, S. Gascon, S.K. Hatzios, V.E. Kagan, K. Noel, X. Jiang, A. Linkermann, M.E. Murphy, M. Overholtzer, A. Oyagi, G.C. Pagnussat, J. Park, Q. Ran, C.S. Rosenfeld, K. Salnikow, D. Tang, F.M. Torti, S.V. Torti, S. Toyokuni, K.A. Woerpel, D.D. Zhang, Ferroptosis: a regulated cell death nexus linking metabolism, redox biology, and disease, Cell 171 (2017) 273–285, https://doi.org/10.1016/j.cell.2017.09.021.

[37] G. Miotto, M. Rossetto, M.L. Di Paolo, L. Orian, R. Venerando, A. Roveri, A.M. Vuckovic, V. Bosello Travain, M. Zaccarin, L. Zennaro, M. Maiorino, S. Toppo, F. Ursini, G. Cozza, Insight into the mechanism of ferroptosis inhibition by ferrostatin-1, Redox Biol. 28 (2020), 101328, https://doi.org/10.1016/j.redox.2019.101328.

[38] C.D. Georgiou, K. Grintzalis, G. Zervoudakis, I. Papapostolou, Mechanism of Coomassie brilliant blue G-250 binding to proteins: a hydrophobic assay for nanogram quantities of proteins, Anal. Bioanal. Chem. 391 (2008) 391–403, https://doi.org/10.1007/s00216-008-1996-x.

[39] F. Curtin, P. Schulz, Multiple correlations and Bonferroni's correction, Biol. Psychiatr. 44 (1998) 775–777, https://doi.org/10.1016/s0006-3223(98)00043-2.

[40] H. Sies, Hydrogen peroxide as a central redox signaling molecule in physiological oxidative stress: oxidative eustress, Redox Biol. 11 (2017) 613–619, https://doi.org/10.1016/j.redox.2016.12.035.

[41] N.C. Andrews, Disorders of iron metabolism, N. Engl. J. Med. 341 (1999) 1986–1995, https://doi.org/10.1056/NEJM199912233412607.

[42] X. Fan, A. Li, Z. Yan, X. Geng, L. Lian, H. Lv, D. Gao, J. Zhang, From iron metabolism to ferroptosis: pathologic changes in coronary heart disease, Oxid. Med. Cell. Longev. 2022 (2022), 6291889, https://doi.org/10.1155/2022/6291889.

[43] T. Morita, Heme oxygenase and atherosclerosis, Arterioscler. Thromb. Vasc. Biol. 25 (2005) 1786–1795, https://doi.org/10.1161/01.ATV.0000178169.95781.49.

[44] A. Pinard, G.T. Jones, D.M. Milewicz, Genetics of thoracic and abdominal aortic diseases, Circ. Res. 124 (2019) 588–606, https://doi.org/10.1161/CIRCRESAHA.118.312436.

[45] J. Shi, Q.H. Wang, X. Wei, B. Huo, J.N. Ye, X. Yi, X. Feng, Z.M. Fang, D.S. Jiang, M.J. Ma, Histone acetyltransferase P300 deficiency promotes ferroptosis of vascular smooth muscle cells by activating the HIF-1alpha/HMOX1 axis, Mol. Med. 29 (2023) 91, https://doi.org/10.1186/s10020-023-00694-7.

[46] M. Edvinsson, N.G. Ilback, P. Frisk, S. Thelin, C. Nystrom-Rosander, Trace element changes in thoracic aortic dissection, Biol. Trace Elem. Res. 169 (2016) 159–163, https://doi.org/10.1007/s12011-015-0432-2.

[47] N. Li, X. Yi, Y. He, B. Huo, Y. Chen, Z. Zhang, Q. Wang, Y. Li, X. Zhong, R. Li, X.H. Zhu, Z. Fang, X. Wei, D.S. Jiang, Targeting ferroptosis as a novel approach to alleviate aortic dissection, Int. J. Biol. Sci. 18 (2022) 4118–4134, https://doi.org/10.7150/ijbs.72528.

[48] Y. Chen, X. Yi, B. Huo, Y. He, X. Guo, Z. Zhang, X. Zhong, X. Feng, Z.M. Fang, X.H. Zhu, X. Wei, D.S. Jiang, BRD4770 functions as a novel ferroptosis inhibitor to protect against aortic dissection, Pharmacol. Res. 177 (2022), 106122, https://doi.org/10.1016/j.phrs.2022.106122.

[49] M. Yang, H. Luo, X. Yi, X. Wei, D.S. Jiang, The epigenetic regulatory mechanisms of ferroptosis and its implications for biological processes and diseases, MedComm (2023) e267, https://doi.org/10.1002/mco2.267, 2020) 4.

[50] W. Song, J. Chen, L. Wei, Ferroptosis in aortic dissection: cause or effect? Pharmacol. Res. (2022), 106344 https://doi.org/10.1016/j.phrs.2022.106344.

[51] Y. Yu, Y. Yan, F. Niu, Y. Wang, X. Chen, G. Su, Y. Liu, X. Zhao, L. Qian, P. Liu, Y. Xiong, Ferroptosis: a cell death connecting oxidative stress, inflammation and cardiovascular diseases, Cell Death Dis. 7 (2021) 193, https://doi.org/10.1038/s41420-021-00579-w.

[52] Y. Chen, Z.M. Fang, X. Yi, X. Wei, D.S. Jiang, The interaction between ferroptosis and inflammatory signaling pathways, Cell Death Dis. 14 (2023) 205, https://doi.org/10.1038/s41419-023-05716-0.
[53] S.E. Corcoran, L.A. O'Neill, HIF1alpha and metabolic reprogramming in inflammation, J. Clin. Invest. 126 (2016) 3699–3707, https://doi.org/10.1172/JCI84431.
[54] G. Lian, X. Li, L. Zhang, Y. Zhang, L. Sun, X. Zhang, H. Liu, Y. Pang, W. Kong, T. Zhang, X. Wang, C. Jiang, Macrophage metabolic reprogramming aggravates aortic dissection through the HIF1alpha-ADAM17 pathway(☆), EBioMedicine 49 (2019) 291–304, https://doi.org/10.1016/j.ebiom.2019.09.041.
[55] W. Liu, W. Zhang, T. Wang, J. Wu, X. Zhong, K. Gao, Y. Liu, X. He, Y. Zhou, H. Wang, H. Zeng, Obstructive sleep apnea syndrome promotes the progression of aortic dissection via a ROS- HIF-1alpha-MMPs associated pathway, Int. J. Biol. Sci. 15 (2019) 2774–2782, https://doi.org/10.7150/ijbs.34888.